Supporting Information

Hierarchical Architecture of Metallic $VTe_2/Ti_3C_2T_x$ MXene Heterostructure for Supercapacitor Applications

Sree Raj K A, [1] Narad Barman [2], Sithara Radhakrishnan [1], Ranjit Thapa [2], and Chandra Sekhar Rout*[,1]

[1] *Centre for Nano and Material Science, Jain University, Jain global campus, Jakkasandra, Ramanagaram, Banglore - 562112, India.*

[2] *Department of Physics, SRM University – AP, Amaravati 522 240, Andhra Pradesh, India.*

**Corresponding author: csrout@gmail.com, r.chandrasekhar@jainuniversity.ac.in (CSR);*

Electrochemical Calculations

Three electrode configuration-

Specific capacitance (C_{sp}) from cyclic voltammetry;

$$Csp = \frac{Area\ of\ CV\ curve}{2 * m * \vartheta * \Delta V} \qquad (S1)$$

Where, m is the mass of active material, ν is the scan rate and ΔV is the potential window.

Specific capacitance (C_{sp}) from galvanostatic charge discharge;

$$Csp = \frac{i * \Delta t}{m * \Delta V} \qquad (S2)$$

Where, i is the applied current, Δt is the discharge time.

Charge balance equation;[1]

$$\frac{m_+}{m_-} = \frac{C_- * \Delta V_-}{C_+ * \Delta V_+} \qquad (S3)$$

Specific capacitance (C_{sp}) of ASC from galvanostatic charge discharge;

$$Csp = \frac{i * \Delta t}{m * \Delta V} \qquad (S4)$$

Energy density of ASC;

$$E_D = \frac{1}{2}CV^2 \tag{S5}$$

Where, C is specific capacitance of ASC, V is the working window of ASC.

Power density of ASC;

$$P_D = \frac{E_D}{\Delta t} \tag{S6}$$

Supporting Figures

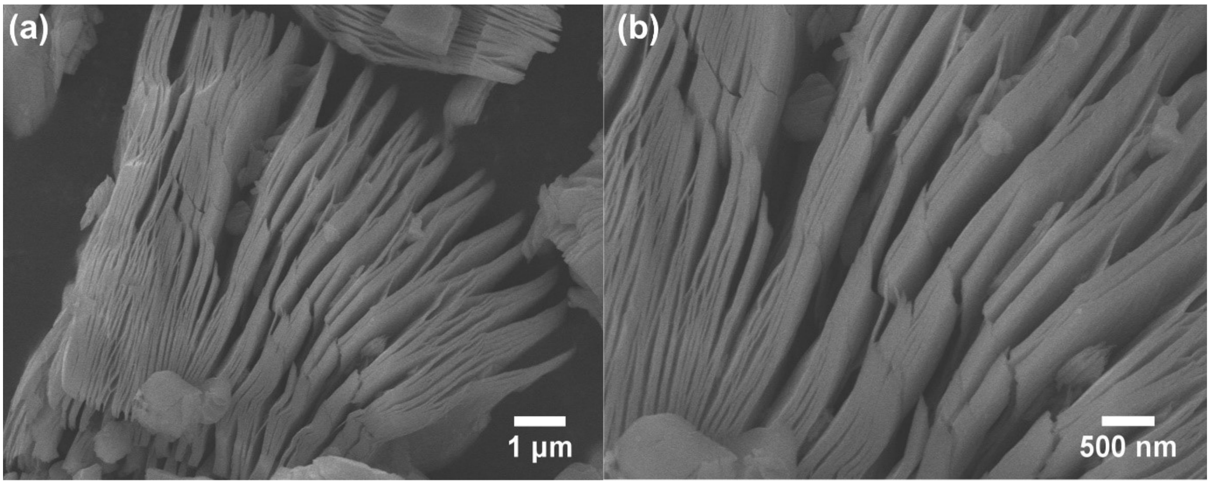

Figure S1: Low (a) and high (b) resolution FESEM images of etched MXene showing the accordion like morphology.

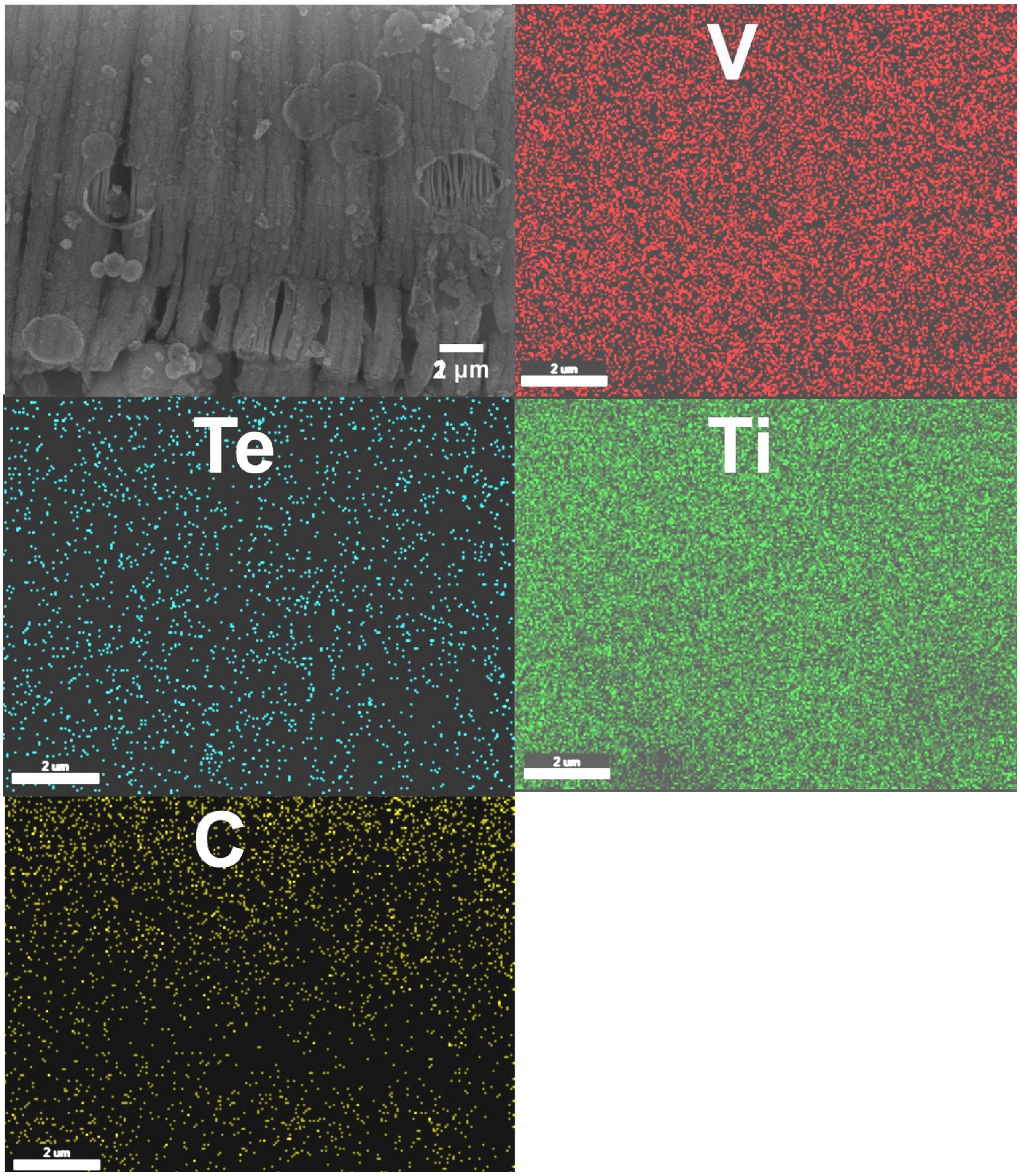

Figure S2: EDS element mapping of VTX80 sample showing the uniform distribution of V, Te, Ti, and C.

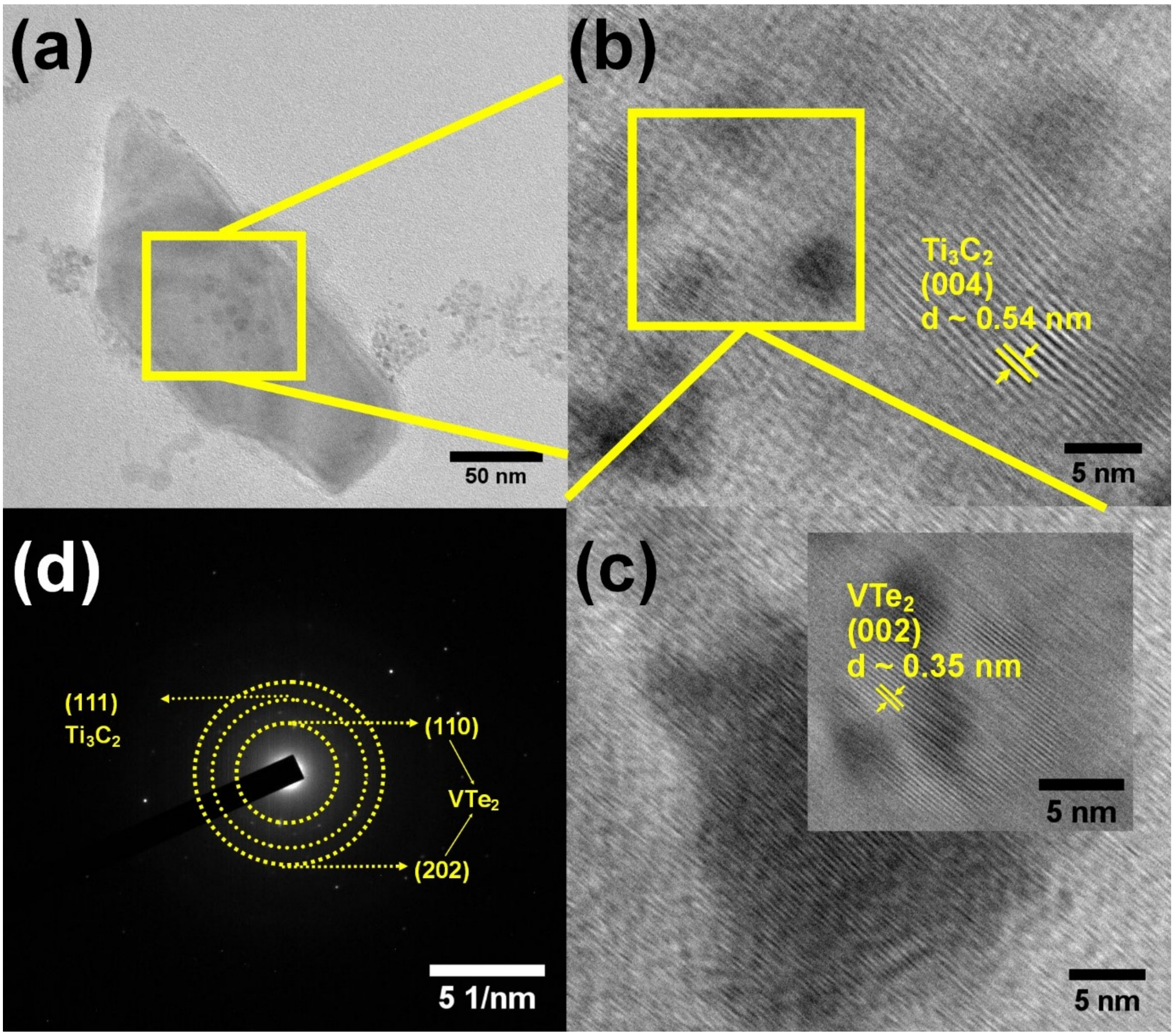

Figure S3: (a) TEM image of VTX 80, (b, c) HRTEM images of VTX 80 showing lattice fringes of (004) plane of Ti_3C_2 MXene and (002) plane of VTe_2 and (d) corresponding SAED pattern.

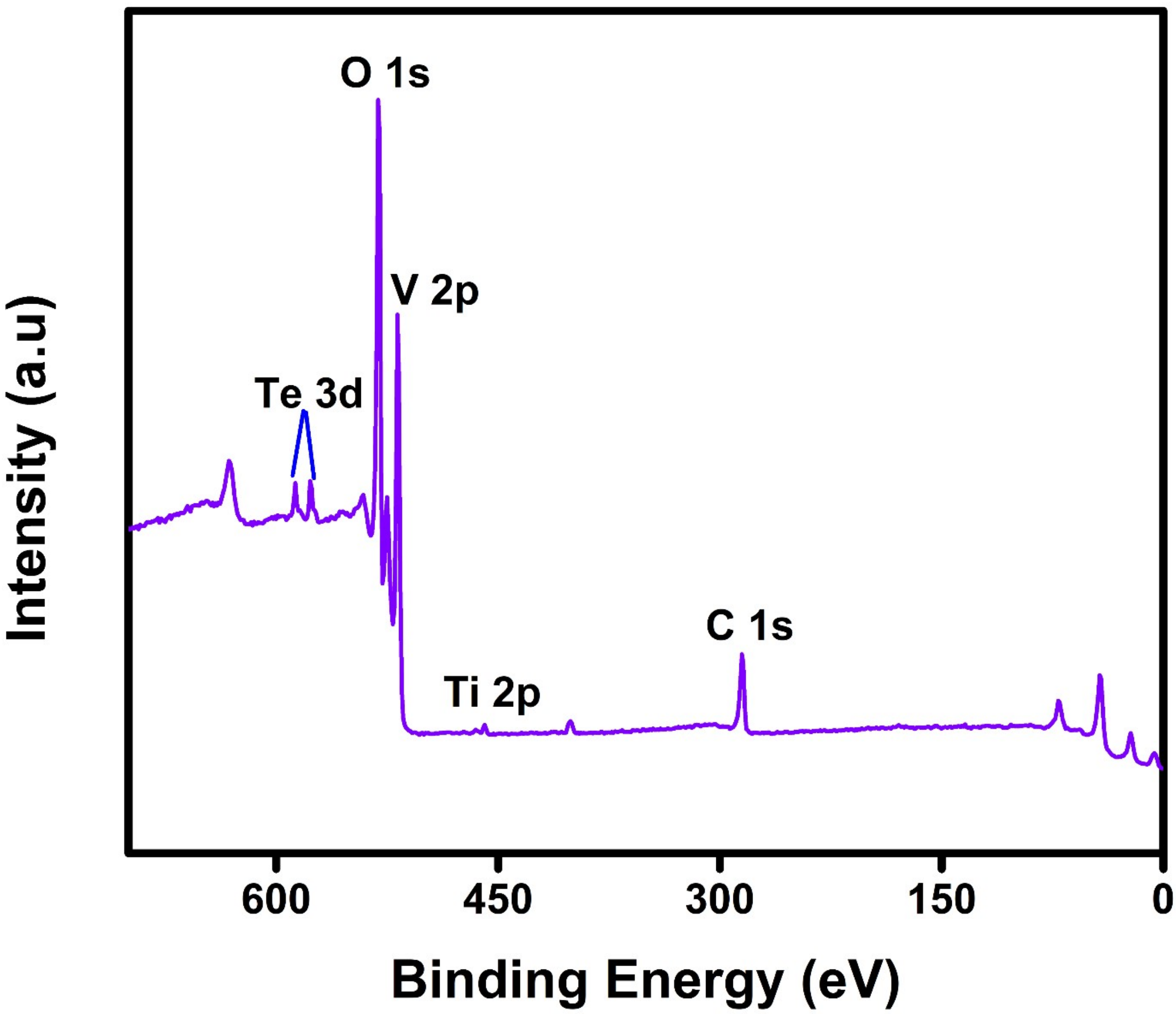

Figure S4: XPS survey spectrum of VTX80 showing the presence of V 2p, Te 3d. C 1s and Ti 2p species.

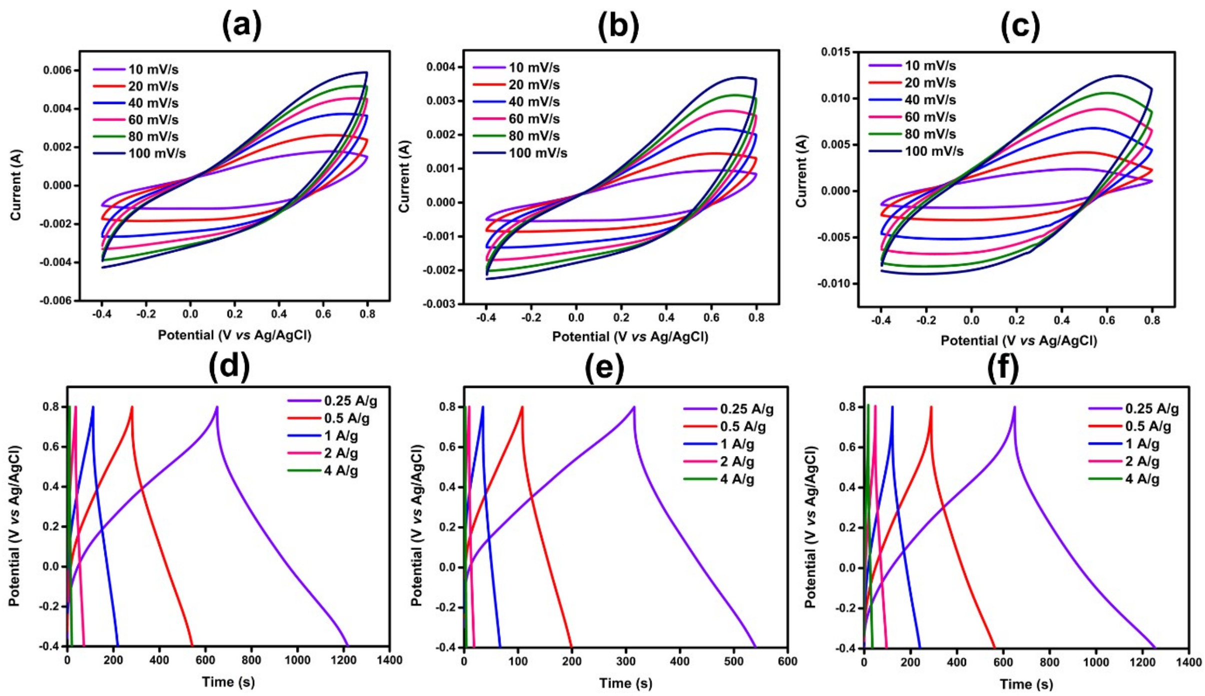

Figure S5: Cyclic voltammograms of (a) VTe_2, (b) VTX40, (c) VTX120 in varying scan rates, GCD curves of (d) VTe_2, (e) VTX40 and (f) VTX120 in different specific currents ranging from 0.25 to 4 A/g.

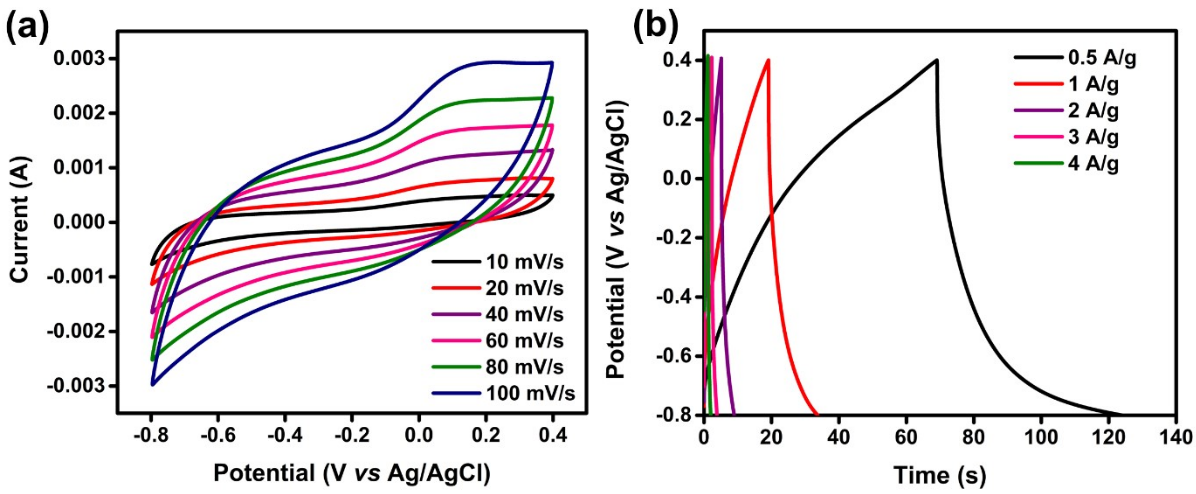

Figure S6: (a) Cyclic voltammogram and (b) GCD profile of MXene.

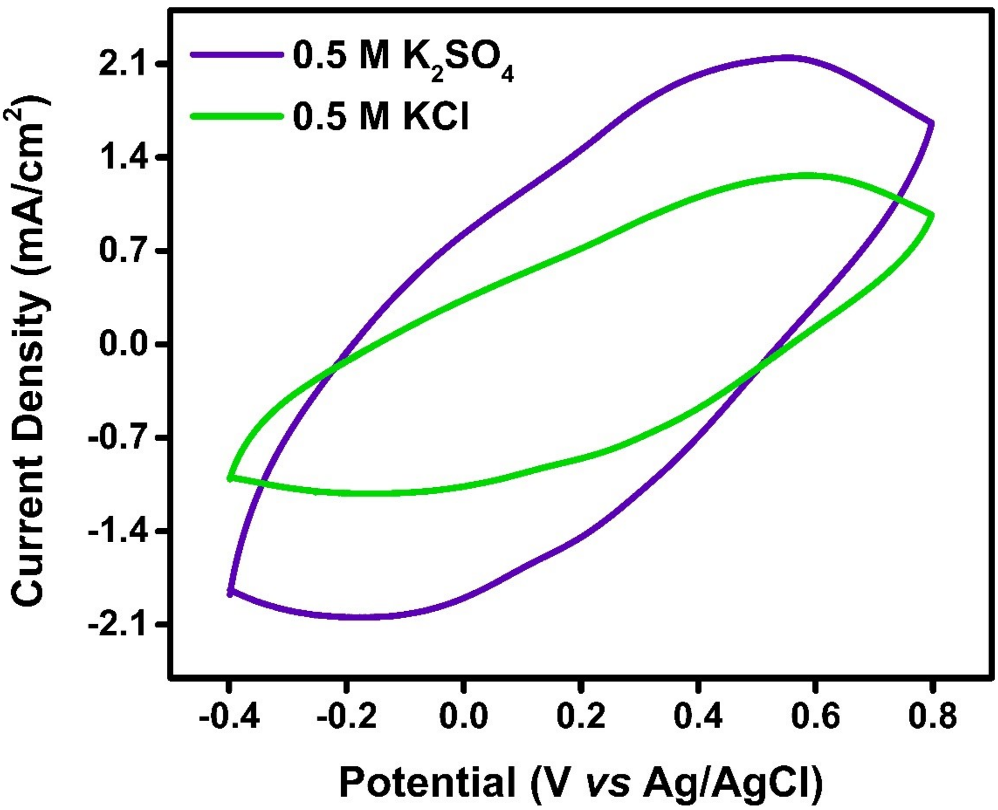

Figure S7: Comparison of the CV curves of VTX80 electrode in 0.5M K_2SO_4 and 0.5M KCl (analysed using a conventional glassy carbo electrode).

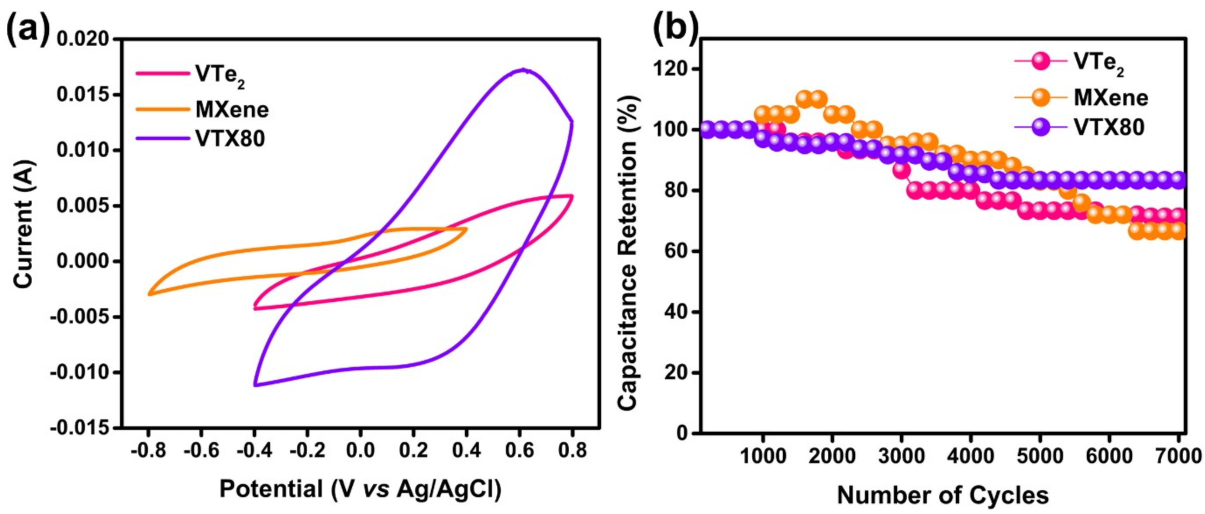

Figure S8: (a) Comparative CV profile of VTe_2, MXene and VTX80 at 100 mV/s, (b) Cyclic stability of VTe_2, MXene and VTX80. VTe_2 and MXene have a cyclic stability of 71.3% and 66.6% respectively, VTX80 on the other hand showed an improved cyclic stability of 83.3%.

Scan Rate (mV/s)	**Capacitive Contribution (%)**	**Diffusive Contribution (%)**
10	81.8	18.2
20	82.9	17.1
40	83.6	16.4
60	85.8	14.2
80	89.2	10.8
100	90.1	9.9
200	97.2	2.8

Table S1: The segregated capacitive and diffusive contributions obtained by deconvoluting CV using Dunn method.

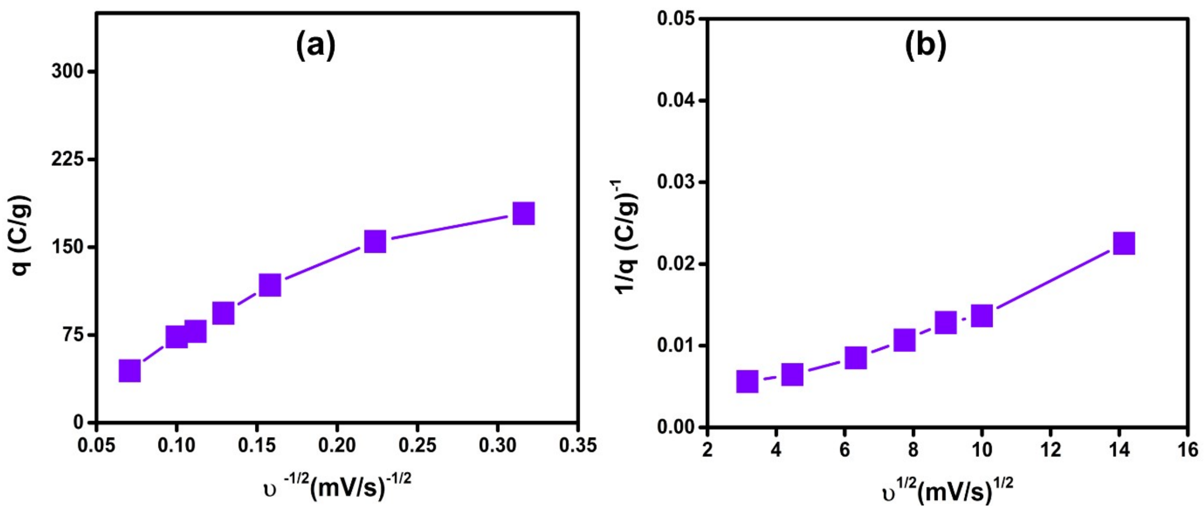

Figure S9: (a-b) Trasatti plots.

Sample	R_s (Ω)	R_{ct} (Ω)
VTe_2	8.07	9.43
VTX40	5.5	18.51
VTX80	2.62	5.48
VTX120	5.11	9.44

Table S2: The R_s and R_{ct} values of all the samples obtained from Nyquist plot.

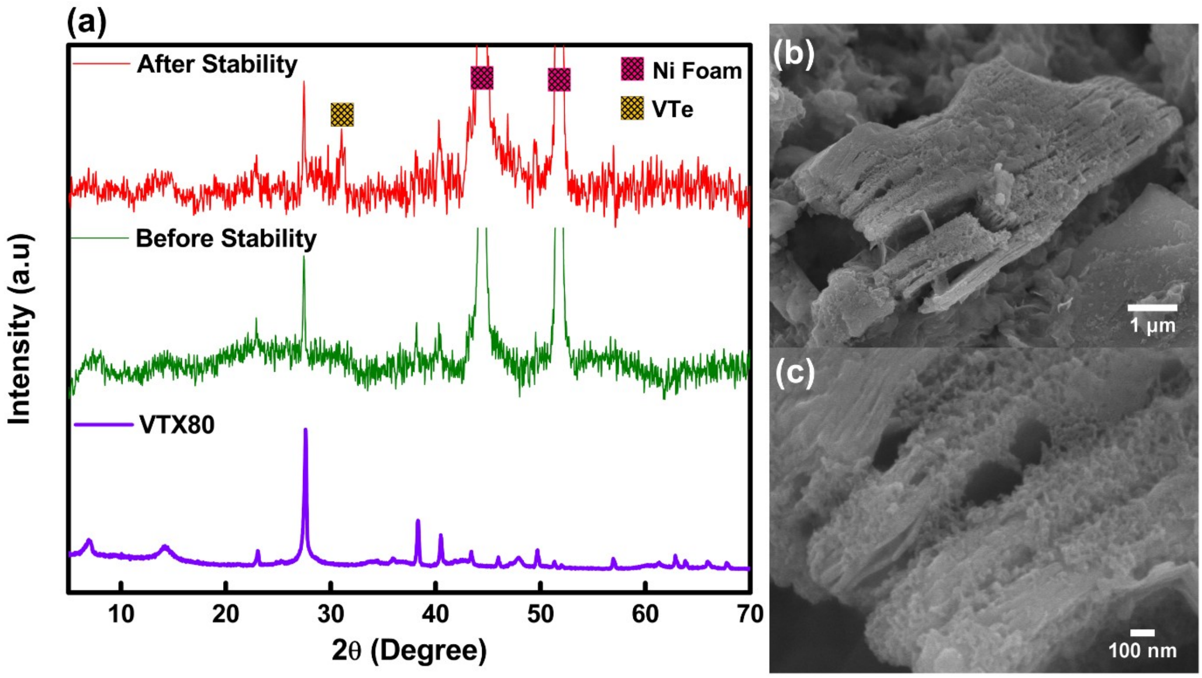

Figure S10: Characterization of VTX80 electrode after electrochemical analysis. (a) XRD pattern of VTX80 electrode before and after. A notable peak ~31° which can be assigned to the (101) plane of VTe (JCPDS: 89-7104). XRD pattern of VTX80 electrode shows sharp intense doublet of Ni foam which has been used as the current collector.[2] (a) low and (b) high resolution FESEM images of VTX80 electrode after the electrochemical analysis. The 3D interconnected structure of VTe_2 and MXene is intact after the electrochemical analyses.

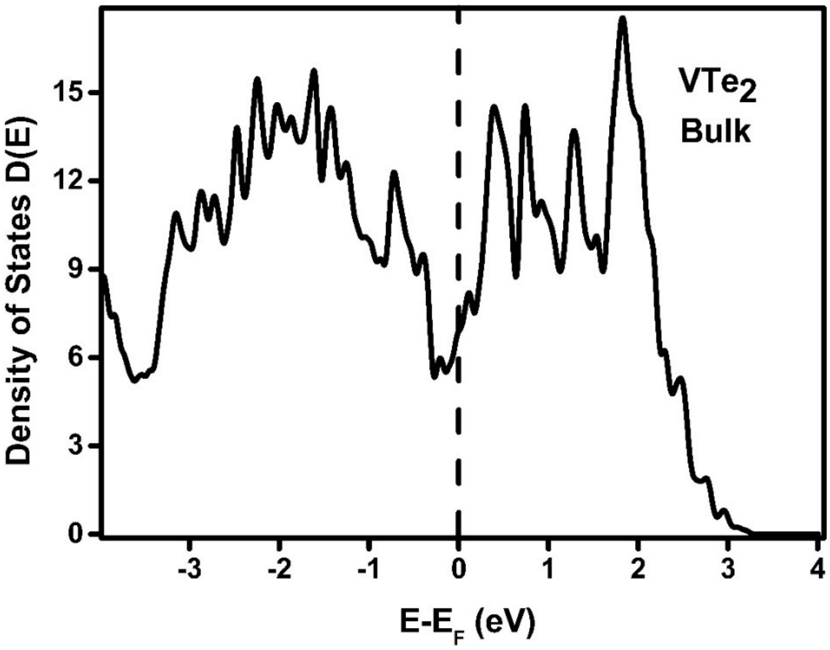

Figure S11: Plot of total density of states of VTe_2 bulk.

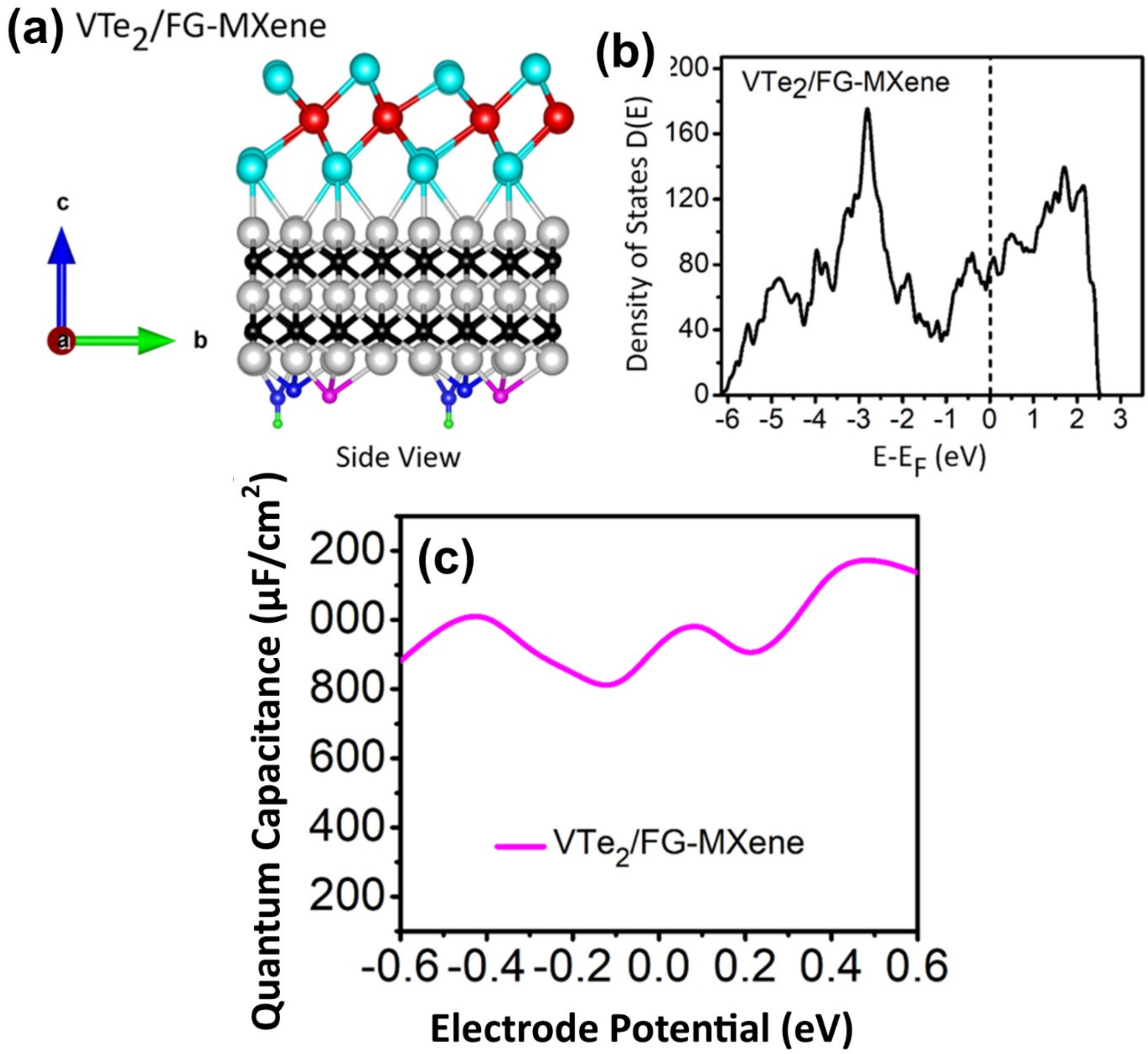

Figure S12: (a) Optimized structure of VTe_2/FG-MXene, (b) total DOS for the proposed model heterostructure and (c) Variation of quantum capacitance against applied electrode potential. Blue, green and pink spheres denote the oxygen, hydrogen and fluorine atoms respectively.

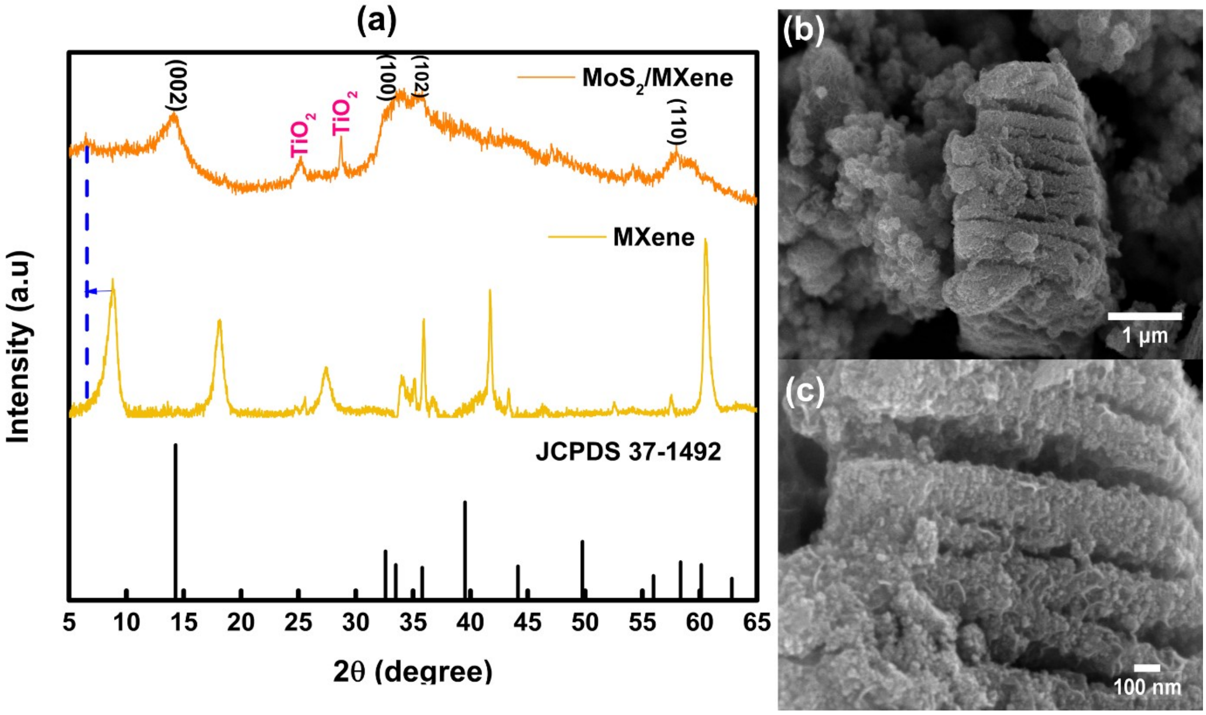

Figure S13: Characterization of the synthesized MoS_2/MXene heterostructure used as the negative electrode. (a) The XRD pattern of MoS_2/MXene heterostructure showed XRD reflections corresponds to the JCPDS card 37-1492 of MoS_2.[3] The (002) peak of Ti_3C_2 MXene has shifted from 8.8° to 6.4° indicating an increment in the interlayer spacing for the heterostructure similar to VTe_2/MXene heterostructure.[4] The presence of TiO_2 is observed in the heterostructure is due to the surface oxidation of MXene.[5] (b, c) FESEM images of MoS_2/MXene reveals a 3D interconnected heterostructure similar to VTe_2/MXene. It clear from the FESEM images that MXene is acting as the growth template for the growth of MoS_2 nanosheets.[6]

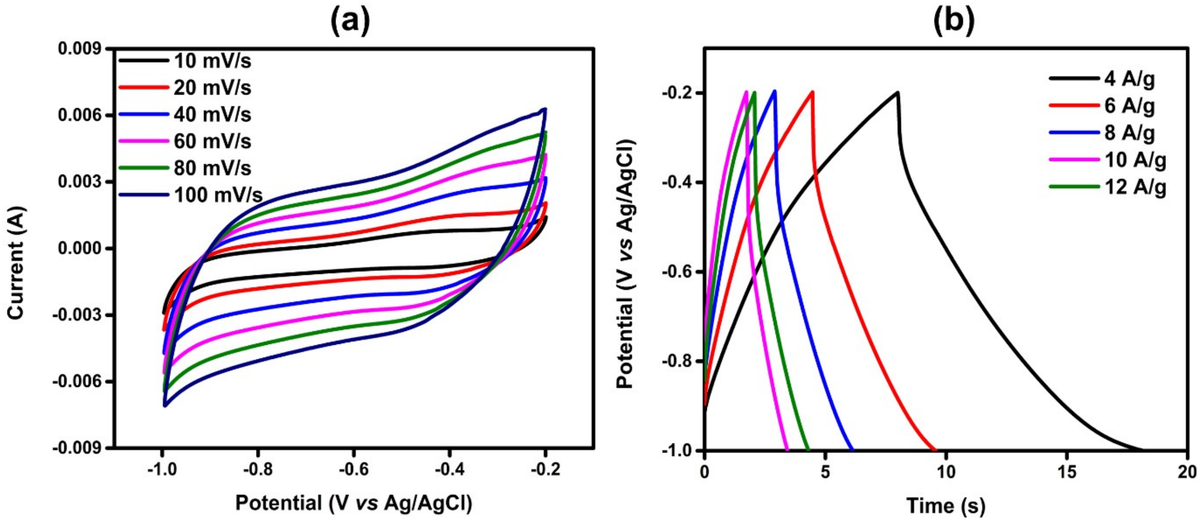

Figure S14: Three electrode measurements of MoS_2/MXene heterostrcture (a) cyclic voltammogram of MoS_2/MXene performed in a potential window of -0.2 - -1.0 V in different scan rates and (b) GCD curves of MoS_2/MXene in varying specific currents.

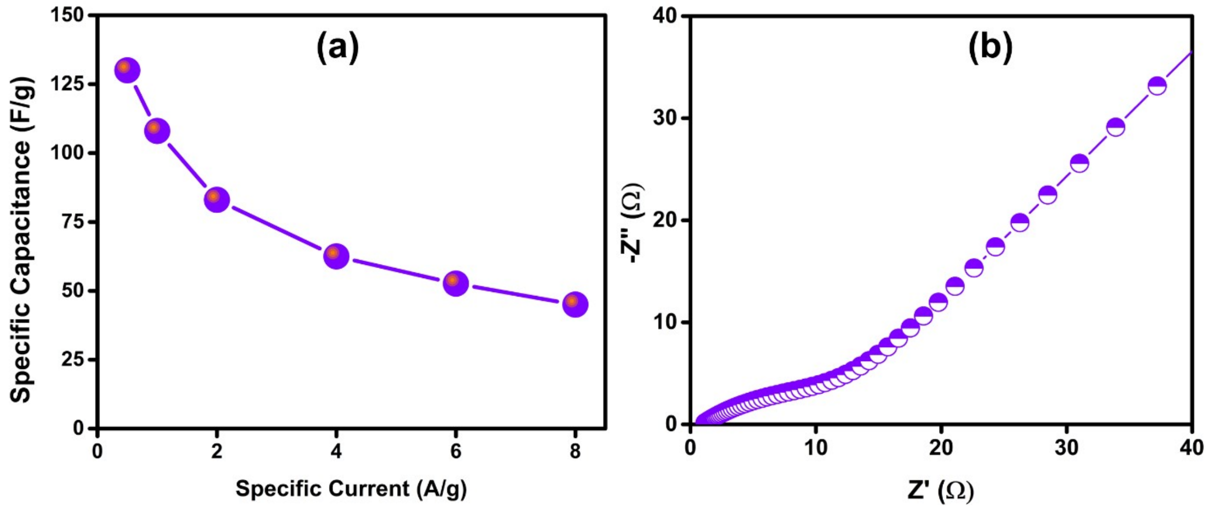

Figure S15: (a) Specific capacitance vs specific current plot of the ASC and (b) Nyquist plot of the ASC.

References

1 Y. Shao, M. F. El-Kady, J. Sun, Y. Li, Q. Zhang, M. Zhu, H. Wang, B. Dunn and R. B. Kaner, *Chem. Rev.*, 2018, **118**, 9233–9280.

2 S. R. K A, S. Adhikari, S. Radhakrishnan, P. Johari and C. S. Rout, *Nanotechnology*,

2022, **33**, 295703.

3 B. Kirubasankar, M. Narayanasamy, J. Yang, M. Han, W. Zhu, Y. Su, S. Angaiah and C. Yan, *Appl. Surf. Sci.*, 2020, **534**, 147644.

4 X. Wang, H. Li, H. Li, S. Lin, W. Ding, X. Zhu, Z. Sheng, H. Wang, X. Zhu and Y. Sun, *Adv. Funct. Mater.*, 2020, **30**, 1–11.

5 S. Raj KA, P. Mane, S. Radhakrishnan, B. Chakraborty and C. S. Rout, *ACS Appl. Nano Mater.*, 2022, **5**, 4423–4436.

6 H. Li, X. Chen, E. Zalnezhad, K. N. Hui, K. S. Hui and M. J. Ko, *J. Ind. Eng. Chem.*, 2020, **82**, 309–316.